Molecular dynamics calculations of infrared absorption spectra in the canonical ensemble: H on Si(100)

1989 J. Phys.: Condens. Matter 1 4129

(http://iopscience.iop.org/0953-8984/1/26/009)

J. Phys.: Condens. Matter 1 (1989) 4129–4140. Printed in the UK

Molecular dynamics calculations of infrared absorption spectra in the canonical ensemble: H on Si(100)

F Ladouceur†, A Selmani†, C Tannous† and G Spronken‡

† Groupe des Couches Minces (GCM), Département de Génie Physique, Ecole Polytechnique, Montréal, Québec, Canada H3C 3A7

‡ Département de Génie Physique, Ecole Polytechnique, Montréal, Québec, Canada H3C 3A7

Received 11 October 1988, in final form 20 December 1988

Abstract. The infrared absorption spectrum of a hydrogenated Si(100)2 × 1 surface is calculated with a constant-temperature molecular dynamics technique (Nosé dynamics). The equations of motion embody radial and angular forces between Si atoms, encompassing previous calculations based on force constants. A novel pair potential determined by *ab initio* quantum chemistry techniques is used for the interactions between H and Si atoms. The spectra obtained, free of any adjustable parameters, compare well with experiment and with previous numerical works modulo a shift of 200 cm^{-1} towards low frequencies. This was noticed previously by Tully and co-workers. The origin of the shift is investigated in detail.

1. Introduction

Hydrogen interactions with silicon surfaces play an important role in many fields. The H–Si surface is an interesting system [1] for theoretical and experimental studies of the various mechanisms underlying chemisorption processes. Vibrational spectroscopy of clean and hydrogenated silicon surfaces provides elements for understanding thermal and laser-induced dynamical processes at silicon surfaces [2]. In LEED or EELS investigations [3], knowledge of Si–H interactions yields valuable information about the structure of the Si surface and its various reconstruction patterns.

Initially, the purpose of this work was to study the IR spectrum of the hydrogenated Si(100)2 × 1 surface in order to understand the origin of the discrepancies that arose between previous MD calculation and experimental results obtained by Tully and co-workers [4]. A more accurate calculation set-up is built on the basis of three-body potential [5] for the Si atoms and a novel two-body potential for the Si–H surface pairs obtained by quantum chemistry techniques [6] (cf. Appendix 1). The statistical ensemble chosen for the simulation is the constant-temperature ensemble (Nosé ensemble [7]). This choice, we believe, is the most natural in that a continuous energy flow is set up between the surface and the bulk, acting as a heat reservoir.

The advantage of Nosé dynamics over other dynamics lies in the fact that the equations of motion include the temperature dependence in a straightforward way. Hence, no extra forces are added to the dynamics, depending on unknown parameters that have to be determined in order to ensure temperature consistency. In addition,

0953-8984/89/264129 + 12 $02.50

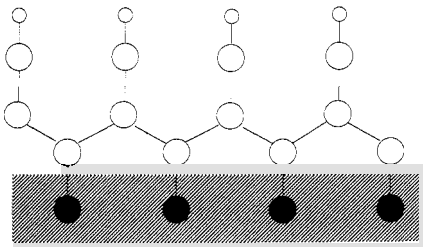

Figure 1. Sketch of a hydrogenated silicon slab. There are three Si layers each containing 16 Si atoms (large circles). The 16 H atoms (small circles) are linked to the first Si layer and the third Si layer has its Si atoms sitting at the crystal positions of the Si(100) plane. The full circles represent the Si atoms of the crystal.

Hoover [8] has also shown that Nosé equations of motion are the only ones compatible with the canonical (constant-temperature) ensemble.

This paper is organised as follows: § 2 contains a detailed description of the system under study, the geometry of the Si(100) surface and the configuration used for the H–Si interaction. In § 3 we describe the equations of motion obtained from the Nosé dynamics method. Section 4 deals with the extraction of IR spectroscopic data from the constant-temperature simulation and the various definitions of the dipole moments we need for calculating the IR absorption. In § 5 we give details of the simulations, and display our results and conclusions in § 6. Finally, the Si–Si potential (taken from the work of Stillinger and Weber [5]) has been used in its separable form following Biswas and Haman [9] in order to reduce the computational effort. A novel Si–H interaction has been generated with quantum chemical methods. Both potentials are discussed in detail in the appendices.

2. Description of the system

Nosé dynamics calculations were carried out for a slab containing 48 silicon (Si) atoms and 16 hydrogen (H) atoms. The configuration of these atoms is sketched in figure 1. A set of 16 H atoms is linked to an uppermost layer of 16 Si atoms. The second and third layers beneath the surface are composed of 16 Si atoms each. The overall slab is 'embedded' in a Si matrix. This is modelled by fixing the Si atoms of the third Si layer at the position occupied by the Si atoms of a crystalline unreconstructed Si(100) surface. The occurrence of non-saturated Si–Si bonds (dangling bonds) on the uppermost layer changes the underlying crystallographic structure significantly. One goes from the bulk, where tetrahedricity of the Si units is respected (diamond structure), to a reconstructed Si surface. The Stillinger–Weber potential predicts a symmetric (2×1) reconstruction for the Si(100) surface [10]. Flat dimer formation [10, 11] is typical of this reconstructed surface sketched in figure 2. It is on this reconstructed surface that the 16 hydrogen atoms were later added for performing the Nosé simulation.

Holding the Si layer in place, however, has an important consequence: the slab is totally disconnected from the bulk, which no longer acts as a heat reservoir. In the Nosé approach, this is overcome by introducing an additional degree of freedom (the proper way of introducing this degree of freedom in the dynamics is explained in § 3) playing the role of damping and random forces such as those arising from the thermal interactions between the atoms of the slab and the heat reservoir. The set of the resulting Nosé equations of motion used in the simulations is given in § 3.

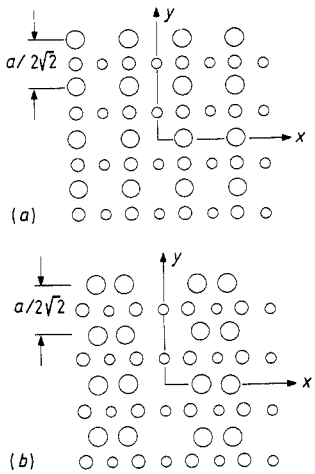

Figure 2. Sketch of (*a*) the unreconstructed Si surface used as the initial configuration of the Si atoms, and (*b*) the reconstructed Si surface obtained from Langevin dynamics simulation. The deeper the atom, the smaller the radius of the circle representing it. In (*a*) and (*b*), $a = 5.43$ Å. The unreconstructed surface has a nearest bond length of 2.35 Å and a second nearest-neighbour distance of 3.84 Å. The first layer of the reconstructed surface has a dimer bond length of 2.41 Å while the other bond lengths have not significantly changed after reconstruction.

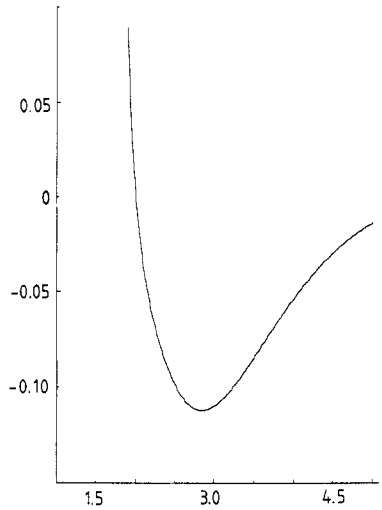

Figure 3. The Si–H potential energy (in hartrees) obtained from quantum chemical techniques as a function of the length of the Si–H bond (in atomic units). 1 au = 1 Bohr radius = 0.529 177 06(44) × 10^{-8} cm; 1 Hartree = 2 Ryd, 1 Ryd = 13.605 804(36) eV.

3. Equations of motion

The procedure used by Nosé [7] to model the system in contact with a heat bath is to introduce a variable, $s(t)$, effecting velocity scaling of all particles such that:

$$\boldsymbol{v}_i(t) = s(t)\,\mathrm{d}\boldsymbol{r}_i/\mathrm{d}t \tag{1}$$

where $\boldsymbol{v}_i(t)$ is the true velocity of particle i and $\boldsymbol{r}_i$ is the solution obtained from the equations of motion. The additional degree of freedom s enters the Lagrangian of the system along with an associated conjugate momentum p_s. From the Lagrangian one obtains, by a Legendre transformation, the following expression for the Hamiltonian [7]:

$$\mathcal{H}(\{\boldsymbol{r}_i\},\{\boldsymbol{p}_i\},s,p_s) = \sum_{i=1}^{N}\frac{|\boldsymbol{p}_i|^2}{2m_i s^2} + V(\{\boldsymbol{r}_i\}) + \frac{p_s^2}{2Q} + (f+1)k_{\mathrm{B}}T\ln s \tag{2}$$

where the $\boldsymbol{p}_i$ are the conjugate momenta of the $\boldsymbol{r}_i$. One has

$$\boldsymbol{p}_i = m_i s^2 \dot{\boldsymbol{r}}_i \tag{3a}$$

$$p_s = Q\dot{s} \tag{3b}$$

In equations (2) and (3*a*), the quantity m_i is the real mass of particle i and the parameter Q, which is determined below, plays the role of inertia for the variable $s(t)$ and controls its time dependence. In equation (2) $V(\{\boldsymbol{r}_i\})$ is the interaction potential which depends

only on the set of individual positions of the particles (i.e., $\{\boldsymbol{r}_i\} = \{\boldsymbol{r}_1, \boldsymbol{r}_2, \ldots, \boldsymbol{r}_N\}$), f is the number of degrees of freedom, k_B is Boltzmann's constant, N is the total number of atoms, and T is temperature. The Hamilton equations yield

$$\dot{\boldsymbol{r}}_i = \boldsymbol{p}_i/m_i s^2 \qquad \dot{\boldsymbol{p}}_i = -\partial V/\partial \boldsymbol{r}_i \qquad \dot{s} = p_s/Q$$
$$\dot{p}_s = \sum_{i=1}^{N} \frac{|\boldsymbol{p}_i|^2}{m_i s^3} - \frac{(f+1)k_B T}{s}. \tag{4}$$

Eliminating conjugate momenta from the above system gives

$$\ddot{\boldsymbol{r}}_i = -(1/m_i s^2)\partial V/\partial \boldsymbol{r}_i - (2\dot{s}/s)\dot{\boldsymbol{r}}_i \tag{5a}$$

and

$$\ddot{s} = \frac{1}{Q}\sum_{i=1}^{N} m_i s|\dot{\boldsymbol{r}}_i|^2 - \frac{(f+1)k_B T}{Qs}. \tag{5b}$$

The fundamental point of the Nosé approach is the equivalence between the microcanonical partition function of the system augmented by the incorporation of the $s(t)$ variable in the dynamics and the canonical partition function of the system exempt from any such additional degree of freedom. The canonical average value of any thermodynamic quantity of interest, G, can thus be computed via the usual expression:

$$\langle G \rangle = \frac{1}{Z}\int \mathrm{d}\Gamma \exp\left(-\frac{\mathcal{H}}{k_B T}\right) G(\Gamma) \tag{6}$$

where Z is the canonical partition function, $\mathcal{H} = \mathcal{H}(\{\boldsymbol{r}_i\}, \{\boldsymbol{p}_i\}, 1, 0)$, Γ represents a classical trajectory in phase space, and the integration is done over all phase space.

The equations of motion for the H atoms are obtained in the following way. Assuming that the uppermost layer of the slab consists of independent Si–H monomers, the equation of motion of a given hydrogen interaction with a companion silicon atom through a pair potential $V_{\text{Si–H}}$ is:

$$\ddot{\boldsymbol{r}}_i = -(1/m_H)\partial V_{\text{Si–H}}/\partial \boldsymbol{r}_i \tag{7}$$

where m_H is the atomic mass of a H atom. The index i refers to the ith hydrogen of 16 interacting with the Si surface. The classical trajectories are obtained from integration of equation (5) and (7) where the Si–Si potential energy, V, is modelled using a modified Stillinger–Weber approach [5] and the two-body potential energy, $V_{\text{Si–H}}$, has been calculated by means of quantum chemistry techniques [6]. The Stillinger–Weber potential embodying a three-body force essential for reproducing the tetrahedral structure of Si entails computation of N^3 terms arising from all $N!/3!(N-3)!$ triplets among N Si atoms. This potential is separable into two-body interactions breaking down the computational number of operations to N^2 per simulation step. This separability is discussed in Appendix 2 after discussion of the pair potential $V_{\text{Si–H}}$ in Appendix 1 (see figure 3). An explicit calculation of the three-body forces as sums of two-body terms is also presented in Appendix 2. The position of each atom can be computed along a given classical trajectory, yielding the dipole moment from which the IR absorption spectrum can be calculated. The precise definitions of the various dipole moments we used are given in § 4.

4. Dipole moments and the IR absorption spectrum

The intensity of the IR absorption spectrum is computed from the expression [12]

$$I(\omega) = \frac{1}{2\pi}\int_{-\infty}^{\infty} \mathrm{d}t\langle \boldsymbol{M}(0)\cdot\boldsymbol{M}(t)\rangle\, \mathrm{e}^{-\mathrm{i}\omega t} \tag{8}$$

where $\boldsymbol{M}(t)$ is the dipole moment vector of the system. Each contribution to the scalar product corresponds to the x, y or z polarisation and the brackets in equation (8) denote the ensemble average. A more practical expression can be obtained from the Wiener–Khintchine theorem yielding the following equivalent expression for the spectrum intensity [13]:

$$I(\omega) = \frac{1}{2\pi}\lim_{T\to\infty}\left(\frac{1}{2T}\sum_{j=x,y,z}\left|\int_{-T}^{T}\mathrm{d}t\, M_j(t)\,\mathrm{e}^{-\mathrm{i}\omega t}\right|^2\right). \tag{9}$$

Two mechanisms are used to compute the dipole moment $\boldsymbol{M}(t)$. The first one is the mechanism proposed in [14] due to deviation from perfect tetrahedricity through stretching of the Si–Si bond. Phenomenological arguments yield the following expression for the resulting dipole moment:

$$\boldsymbol{M}_a = \sum_{k(i,j),i\neq j}(\boldsymbol{r}_{ki}-\boldsymbol{r}_{kj})(\boldsymbol{U}_{ki}\cdot\boldsymbol{r}_{ki}-\boldsymbol{U}_{kj}\cdot\boldsymbol{r}_{kj}) \tag{10}$$

where $k(i,j)$, $i\neq j$ indicates that the sum runs over all the nearest neighbours i and j of atom k such that $i\neq j$, $\boldsymbol{U}_{mn}=\boldsymbol{U}_n-\boldsymbol{U}_m$, where $\boldsymbol{U}_{n(m)}$ is the displacement vector of the atom $n(m)$ from its equilibrium position, and $\boldsymbol{r}_{nm}$ is the unit vector between the equilibrium positions of the atoms n and m. The scalar products on the RHS of equation (7) represent compressed (negative scalar product) or extended (positive scalar product) bonds. Actually, expression (10) refers to the dipole moment resulting from the charge rearrangement from extended to compressed bonds. The contribution of the bending (or wagging) modes, however, gives an expression of the dipole moment which is more sensitive to angular distortions betwen adjacent Si–Si bonds, resulting in a deviation from perfect tetrahedricity. The mechanism of Winer [15] provides such an expression. One has

$$\boldsymbol{M}_b = \sum_{k(i,j),i\neq j}(\boldsymbol{r}_{ki}+\boldsymbol{r}_{kj})(\boldsymbol{U}_{ki}\cdot\boldsymbol{r}_{kj}+\boldsymbol{U}_{kj}\cdot\boldsymbol{r}_{ki}). \tag{11}$$

It is easily shown that (i) two terms with the same indices of equations (10) and (11) are mutually perpendicular, and (ii) both expressions (i.e., $\boldsymbol{M}_a$ and $\boldsymbol{M}_b$) vanish identically in the case of pure crystalline Si (perfect tetrahedral diamond structure). They are convenient expressions accounting for the contribution to the stretching and bending modes of the IR absorption.

5. Details of the simulation

Periodic boundary conditions in the xy plane (the direction z is along the normal to the surface of the system) are used to eliminate edge effects. The upper surface is assumed to be free while the Si atoms of the bottom Si layer are held fixed to the position of the Si bulk atoms in the (100) plane. The linear dimension of the cell is 15.358 Å. The quasi-classical temperature obtained from the expression [4]:

$$T_{\mathrm{QC}} = \frac{\hbar\omega_{\mathrm{D}}}{k_{\mathrm{B}}}\left(\frac{1}{2}+\frac{\exp(-\hbar\omega_{\mathrm{D}}/k_{\mathrm{B}}T)}{1-\exp(-\hbar\omega_{\mathrm{D}}/k_{\mathrm{B}}T)}\right) \tag{12}$$

where $\hbar$ is Planck's constant divided by 2π and ω_{D} is the Debye frequency taken to

be 500 cm^{-1} [10], is T_{QC} = 330 K for all simulations (this corresponds to the classical temperature T = 100 K). The integration time-step is 7.5×10^{-4} ps, and a typical Nosé dynamics simulation takes up 40000 time-steps. Simple dimensional analysis arguments show that the parameter Q occurring in equations (2), (3*b*), (4), and (5*b*) is of the order of

$$Q \sim t_s^2(f+1)k_B T_{QC} \tag{13}$$

where t_s is a characteristic time of a few picoseconds. A first simulation is carried out without the hydrogen atoms until an equilibrium configuration is reached. The starting configuration is sketched in figure 2(*a*). The nearest-neighbour bond length is 2.35 Å while the second-neighbour distance is 3.84 Å (Si(100) unreconstructed surface). The system is then set to evolve under the action of the Si–Si interaction until equilibrium is reached (the temperature is set to T_{QC} = 330 K). It appears from our study and that of Weber [10] that perfect reconstruction is very sensitive to the initial positions and velocities. These may be chosen arbitrarily such that a perfect Si(100)2 × 1 reconstruction is obtained. Since the reconstruction time is a long process as far as molecular dynamics (MD) is concerned, one has to use a method such as that of steepest-descent [10] or a stochastic (Langevin) integration scheme (which strongly perturbs the initial surface by the action of random forces) in order to obtain the reconstructed surface in a reasonable time. Since we are not interested in the process of reconstruction as such, but rather in the IR absorption spectrum, we therefore used a starting configuration for the Si atoms obtained from Langevin simulation [6, 16] and proceeded from there. This yielded the Si(100)2 × 1 reconstructed surface of figure 2(*b*) whose parameters are in good agreement with those obtained by Weber [10] (see also Abraham and Batra [11] and Lucchese and Tully [4]). The average distance between two Si atoms in a given dimer is 2.41 Å, while the bond length between atoms in the first and second layers is left unchanged. Actually, the displacements of the atoms during reconstruction are somewhat smaller than those observed previously [4].

The hydrogen atoms are introduced once thermal equilibrium is reached. In fact, these atoms are introduced such that they form 16 individual Si–H bonds with the Si atoms of the upper surface of the reconstructed Si(100)2 × 1 surface. The equations of motion (5) are integrated by a modified second-order predictor-corrector [17] and the dipole moments $\boldsymbol{M}_a$ and $\boldsymbol{M}_b$ (cf. equations (10) and (11)) are computed along the classical trajectory. The use of equation (9), together with the fast Fourier transform technique, then yields the absorption spectrum.

6. Results

We adopt the following nomenclature for the spectra obtained. Those obtained from the Alben *et al* [14] formula and due to bond-stretching absorption are called *R*-type dipole moments $\boldsymbol{M}_a$ (equation (10)), whereas those obtained from Winer [15] formula ane due to bond-bending absorption dipole moments $\boldsymbol{M}_b$ (equation (11)) are called Θ-type.

Before the surface is hydrogenated, one has to verify that no absorption will occur at the clean surface for the frequency range 2000–2500 cm^{-1}, as confirmed experimentally [4].

Once this check is successful, we are ready to explore the 2000–2500 cm^{-1} region which is of experimental interest since it has been studied accurately with high-resolution techniques [4], and the check serves for calibrating the apparatus and checking the

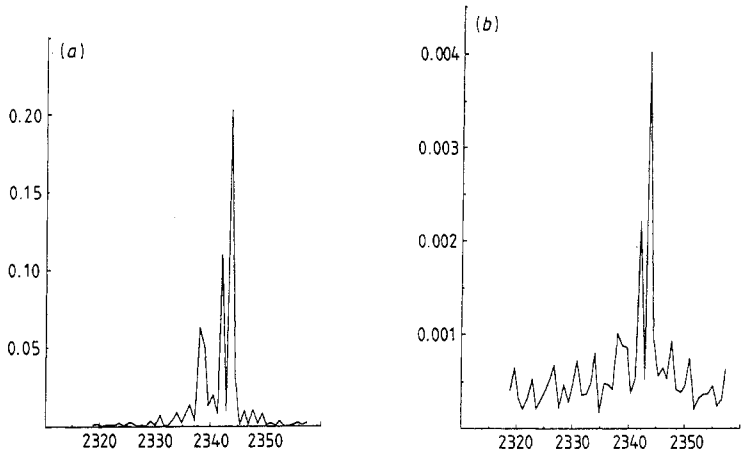

Figure 4. Infrared absorption spectrum (arbitrary units) of the hydrogenated Si(100)2 × 1 surface as a function of frequency (in cm^{-1}) in the range 2310–2360 cm^{-1}; (*a*) using M_a as diopole moment, (*b*) using M_b. In both cases, the total simulation time is 40 ps.

nature of the surface to be studied since it is known that no absorption should occur for the clean surface in this frequency range. Any absorption in this region, after the addition of H, is due solely to the interactions between H and the Si surface.

In figure 4(*a*) the *R*-spectrum is displayed for the hydrogen-covered Si(100)2 × 1 surface in the region of experimental interest. The corresponding Θ-spectrum shown in figure 4(*b*) shows the same features present in the *R*-spectrum at almost the same frequency values. Both spectra show the Si–H antisymmetric stretch at 2338 cm^{-1} and the Si–H symmetric stretch at 2343 cm^{-1} peaks. Two comments are in order, however. First, the magnitude of the intensity observed in the Θ-spectra in the range 2000–2500 cm^{-1} is always much weaker than the corresponding one in the *R*-spectra because of the relative angular stiffness of the Si–H bond. Second, the large peak consisting of two components differs slightly from those measured experimentally and obtained by microcanonical ensemble molecular dynamics techniques or Langevin simulations by Tully and co-workers [4].

Here again, as in [4], the spectrum must be shifted by ~200 cm^{-1} towards lower frequencies in order to achieve good agreement with experimental results. This fact was predictable since a linearisation around the minimum of the Si–H potential gives a resonance frequency of 2320 cm^{-1} when one takes into account the reduced mass of the Si–H system. It should be noted here that, since the Si–H potential was obtained accurately with a realistic (100) silicon surface, there must exist a physical mechanism that explains this shift. Hence, it is doubtful that a 10% uncertainty on the potential coefficients would account in both our case and that of Tully and co-workers for the 200 cm^{-1} shift, as stated in [4].

The origin of this shift is not due to our neglect of dipole–dipole interactions between the Si–H bonds since the largest dipole–dipole interaction is the order of 3 cm^{-1} (see Chabal and Raghavachari [18]). It is worth noting that the results presented here are typical: different total simulation times and trajectories in phase space (cf equation (6)) yield only small peak shifts (a few cm^{-1}). An average of these results will not yield the 200 cm^{-1} shift observed experimentally [4]. The origin of this shift is still an open question.

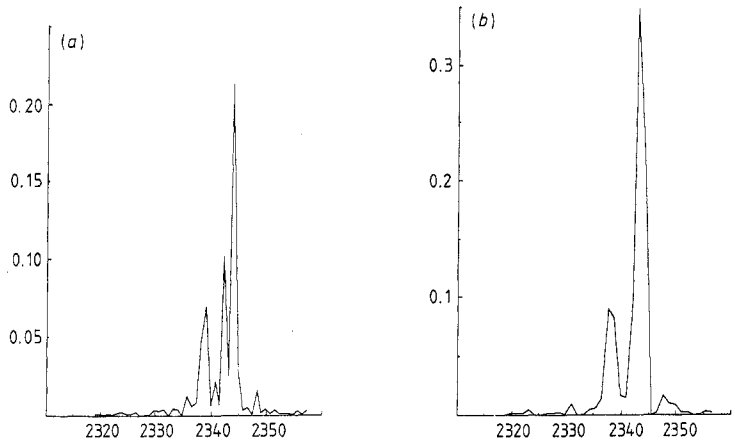

Figure 5. Infrared absorption spectrum (arbitrary units) of the hydrogenated Si(100)2 × 1 surface as a function of the frequency in the range 2310–2360 cm^{-1} using M_a for the dipole moment for two simulation times: (*a*) total simulation time is 35 ps, (*b*) 25 ps.

Furthermore, we believe the Si–H symmetric stretch peak split-off is due to our use of a fully anharmonic pair potential V_{Si-H} in contrast to [4]. By comparing two *R*-spectra (figures 5(*a*), 5(*b*)) at long and short total simulation times corresponding to high and low resolutions, respectively, one can verify that splitting occurred not only in the symmetric stretch peak but also in the antisymmetric stretch lower-frequency peak.

The spectrum of figure 5(*b*) obtained after only 25 ps total simulation time is the one with the closest resemblance to experimental results. Although this might be considered coincidental, one might argue that the same result is likely to be obtained by averaging a number of times the long time simulation results.

Previously, Tully and co-workers [4] interpreted their experimental results with a standard microcanonical molecular dynamics simulation and a Langevin simulation method. Their initial conditions, integration schemes, forces and dipole moments, are basically different from ours. We start from an unreconstructed surface and allow it to reconstruct by itself through the Stillinger–Weber interaction, whereas Tully and co-workers [4] start from the reconstructed surface. In the force calculations we use the Stillinger–Weber three-body interaction between Si atoms and use quantum chemical techniques to determine a novel *ab initio* Si–H interaction potential, whereas Tully and co-workers [4] use a force field for the Si–Si interaction derived from phonon spectra calculation by Tubino and co-workers [19]. Morevoer, Tully and co-workers [4] model the Si–H interaction with diagonal and off-diagonal stretch and bend force constants derived from *ab initio* Hartree–Fock calculations for a Si_2H_6 cluster. On the other hand, the anharmonic interaction potentials we use have the drawback of inducing a fine structure at high resolution in the absorption spectrum.

The ensemble we select is canonical and the equations of motion we integrate are obtained from the Nosé method whereas Tully and co-workers [4] perform the Langevin simulation with Beeman algorithm [20] and the microcanonical ensemble calculation by standard molecular dynamics algorithms.

The dynamic dipole moments used by Tully and co-workers [4] to calculate the IR absorption were extracted from the Si_2H_6 cluster calculation after an enlargement of the basis set and inclusion of additional electron correlation terms. This approach is different

from ours (described in detail in § 4). In conclusion, the present work shows that starting from different models (interaction potentials, dipole moment definitions etc) MD may produce slightly different results as far as it regards spectra which are probably the most time-consuming data to extract from a system at equilibrium, especially when one aims for high-resolution studies. The model we have selected was as realistic and accurate as possible, but was unable to correct the existing discrepancies between MD spectra and experimental ones.

Once the origin of this discrepancy is solved, a possible extension of our work is the case of molecular hydrogen interacting with a crystalline or amorphous Si surface. This is of interest for the understanding of the details of the bonding between H and Si and may explain surface kinetics effects at the origin of water dissociation on silicon surfaces or the microscopic origin of light-induced changes in a-Si : H [21].

Acknowledgments

We wish to thank F H Stillinger for providing numerical data on the Si–Si potential and R Biswas for helpful comments. We also thank J-Y Harbec, L Lewis, E Sacher, D Salahub and A Yelon for various discussions. CT especially thanks Y Chabal and J C Tully for enlightening discussions and constructive criticism. FL would like to thank Jean Berger for his friendliness. CT acknowledges support from the 'Programme expérimental de soutien à l'emploi scientifique' of the Ministère de l'éducation du Québec. This work benefited from various individual and team grants originating from the Conseil de recherches en sciences naturelles et en génie (CRSNG) and Fonds FCAR du Québec.

Appendix 1

In order to model the H–Si (100) interaction, we take a cluster of 11 Si atoms large enough to account for the effects of nearest neighbours on this interaction. The unreconstructed (100) uppermost face consists of five Si atoms among which the central one is to be the adsorption site of the hydrogen atom. The latter is approaching the surface along the normal to the surface above the central uppermost Si. The other surrounding Si atoms are saturated by hydrogens and occupy the same position as in the crystal.

The total energy calculations were done with a linear combination of Gaussian-type orbitals–local spin density (LCGTO-LSD) method. This method is based on Dunlap's LCAO–X_α method [22] with an exchange correlation potential of the Vosko–Wilk–Nusair type [23]. The interaction potential between H and a single Si belonging to the surface is extracted from three different total energies:

$$V_{\text{H-Si}}(r) = E_{\text{T}}(r) - E_{\text{T}}^{\text{c}}(r) - E_{\text{H}} \tag{A1.1}$$

where $E_{\text{T}}(r)$ is the total energy of the silicon cluster with H adsorbed at a height r above the surface. The second term on the RHS of equation (A1.1) is the total energy of the cluster without H but with a fictitious atom having zero electrons, located at the same height as the adsorbed hydrogen (H_{ads}) and described by the same basis set as H_{ads}. This is done in order to reduce basis superposition effects on the calculation of $V_{\text{H-Si}}(r)$. Finally, E_{H} is the total energy of the isolated H atom.

The interaction potential obtained and shown in figure 1 yielded an equilibrium H–Si distance of 2.85 au ($\simeq$1.5 Å), which compares well with the experimental value of 1.48 Å [6]. In addition, the H vibration frequency 2182 cm^{-1} obtained from the curvature

around the minimum of $V_{H\text{-}Si}(r)$ agrees reasonably well with the experimental value of 2095 cm^{-1}.

An accurate polynomial fit to the data obtained for $V_{H\text{-}Si}(r)$ is given by

$$V_{H\text{-}Si}(r) = a_1 + a_2 r^{-1} + a_3 r^{-2} + a_4 r^{-3} + a_5 r^{-4} + a_6 r^{-7} + a_7 r^{-8} \tag{A1.2}$$

where $a_1 = 0.147417$, $a_2 = -5.42700$, $a_3 = 63.16500$, $a_4 = -297.058$, $a_5 = 499.0360$, $a_6 = -2156.29$ and $a_7 = 2462.380$. The units are such that r is expressed in atomic units and $V_{H\text{-}Si}(r)$ in hartrees.

The χ_2 test for the fit yields a value of 0.756×10^{-5}. Note that other functional forms were tested such as Morse or Rydberg type [24]. The χ^2 test value was always higher than the present one. Besides, the polynomial form of $V_{H\text{-}Si}(r)$ allows a fast calculation of the forces in the simulation.

Appendix 2

The potential energy of the Si–Si bond has two- and three-body contributions. One has

$$V = \sum_{i<j} V_2(\boldsymbol{r}_i, \boldsymbol{r}_j) + \sum_{i<j<k} V_3(\boldsymbol{r}_i, \boldsymbol{r}_j, \boldsymbol{r}_k) \tag{A2.1}$$

where

$$V_2(\boldsymbol{r}_i, \boldsymbol{r}_j) = \varepsilon f_2(\boldsymbol{r}_{ij}/\sigma) \tag{A2.2}$$

with

$$\boldsymbol{r}_{ij} = \boldsymbol{r}_j - \boldsymbol{r}_i \tag{A2.3}$$

and

$$f_2(\boldsymbol{u}) = \begin{cases} A(Bu^{-p} - u^{-q}) \exp[(u-a)^{-1}] & u < a \\ 0 & u \geqslant a \end{cases} \tag{A2.4}$$

In this last expression, $u = |\boldsymbol{u}|$. The values of the parameters ε, A, B, p, q and a are given below. The three-body potential is given by

$$V_3(\boldsymbol{r}_i, \boldsymbol{r}_j, \boldsymbol{r}_k) = \varepsilon f_3(\boldsymbol{r}_i/\sigma, \boldsymbol{r}_j/\sigma, \boldsymbol{r}_k/\sigma) \tag{A2.5}$$

where [11]

$$f_3(\boldsymbol{u}_i, \boldsymbol{u}_j, \boldsymbol{u}_k) = h(u_{ij}, u_{ik}, \theta_{jik}) + h(u_{ji}, u_{jk}, \theta_{ijk}) + h(u_{ki}, u_{kj}, \theta_{ikj}). \tag{A2.6}$$

The auxiliary functions $h(\ldots)$ are given explicitly by

$$h(u_{ij}, u_{ik}, \theta_{jik}) = \begin{cases} \lambda \exp\left(\dfrac{\alpha}{u_{ij} - a} + \dfrac{\alpha}{u_{ik} - a}\right)(\tfrac{1}{3} + \cos\theta_{jik})^2 & u_{ij} \text{ and } u_{ik} < a \\ 0 & \text{otherwise} \end{cases} \tag{A2.7}$$

where θ_{jik} $(=\theta_{kij})$ is the angle between the vectors $\boldsymbol{u}_{ij}$ and $\boldsymbol{u}_{ik}$ and where $u_{nm} = |\boldsymbol{u}_{nm}|$. Note that in the case of the diamond structure, $\frac{1}{3} + \cos\theta_{jik} = 0$. The values of the parameters in equations (A2.2), (A2.4), (A2.5), and (A2.7) are $A = 7.049556277$, $B = 0.6022245584$, $p = 4$, $q = 0$, $a = 1.8$, $\lambda = 21.0$, $\alpha = 1.2$, $\sigma = 2.0951$ Å and $\varepsilon = 3.4723 \times 10^{-19}$ J.

The forces acting on atom n due to two- and three-body potentials are obtained from the gradient of the total potential with respect to the coordinates of the atom in question. One obtains

$$\boldsymbol{F}_n^{(2)} = \frac{\varepsilon}{\sigma} \sum_{j \neq n} \frac{\partial f_2(u_{nj})}{\partial u_{nj}} \hat{\boldsymbol{u}}_{nj} \tag{A2.8}$$

where the unit vector is defined by

$$\hat{\boldsymbol{u}}_{nj} = \boldsymbol{u}_{nj}/u_{nj} = \boldsymbol{r}_{nj}/r_{nj} \tag{A2.9}$$

and, using the separability of the functions $h(\ldots)$,

$$h(u_{ij}, u_{ik}, \theta_{jik}) = g(u_{ij})g(u_{ik})(\tfrac{1}{3} + \cos\theta_{jik})^2$$

one obtains, after lengthy but straightforward algebra,

$$\frac{2\sigma}{\varepsilon}\boldsymbol{F}_n^{(3)} = \sum_k \frac{4\pi}{2k+1} C_k \sum_{m=-k}^{k} \sum_j \{f_{km}(\boldsymbol{u}_{nj})[\vartheta_{km}^{n*} + (-1)^k \vartheta_{km}^{j*}] + \text{cc}\}$$
$$- 4 \sum_k C_k \sum_{j \neq n} g(u_{nj}) \frac{\partial g(u_{nj})}{\partial u_{nj}} \hat{\boldsymbol{u}}_{nj} \tag{A2.10}$$

where $C_0 = \frac{4}{9}$, $C_1 = C_2 = \frac{2}{3}$, and $C_k = 0$ for $k > 2$, and where

$$\vartheta_{km}^i = \sum_{j \neq i} g(u_{ij}) Y_{km}(\theta_{ij}, \varphi_{ij}) \tag{A2.11}$$

$$g(u) = \begin{cases} \sqrt{\lambda}\exp[\alpha/(u-a)] & u < a \\ 0 & \text{otherwise.} \end{cases} \tag{A2.12}$$

$$f_{km}(\boldsymbol{u}_{nj}) = Y_{km}(\hat{\boldsymbol{u}}_{nj}) \frac{\partial g(u_{nj})}{\partial u_{nj}} \hat{\boldsymbol{u}}_{nj} + \frac{g(u_{nj})}{2u_{nj}} \{2im \sin\theta_{nj}\, Y_{km}(\hat{\boldsymbol{u}}_{nj})$$
$$- \mathrm{i}\cos\theta_{nj}[\beta_k^m Y_{km+1}(\hat{\boldsymbol{u}}_{nj})\, \mathrm{e}^{-\mathrm{i}\varphi_{nj}} + \beta_k^{-m} Y_{km-1}(\hat{\boldsymbol{u}}_{nj})\, \mathrm{e}^{\mathrm{i}\varphi_{nj}}]\} \hat{\varphi}_{nj}$$
$$+ \frac{g(u_{nj})}{2u_{nj}} [\beta_k^m Y_{km+1}(\hat{\boldsymbol{u}}_{nj})\, \mathrm{e}^{-\mathrm{i}\varphi_{nj}} - \beta_k^{-m} Y_{km-1}(\hat{\boldsymbol{u}}_{nj})\, \mathrm{e}^{\mathrm{i}\varphi_{nj}}]\theta_{nj} \tag{A2.13}$$

where

$$\beta_k^m = [(k-m)(k+m+1)]^{1/2}$$

and where the notation used for the spherical harmonics is

$$Y_{km}(\hat{\boldsymbol{u}}_{nj}) = Y_{km}(\theta_{nj}, \varphi_{nj}).$$

The unit vectors in equations (A2.8), (A2.10) and (A2.13) are the local spherical unit vectors. The expression (A2.13) was first obtained by Biswas and Hamann [9]. The sign of the first term on the RHS of (A2.13) differs from their expression, however. The second term on the RHS of (A2.13) also differs: one has i times cos θ instead of simply cos θ, as in the corresponding expression of Biswas and Hamann.

The separability of the Stillinger–Weber potential was not exploited previously. By exploiting its separability following the work of Biswas and Hamann [9] the computational effort is reduced to N^2 from N^3, where N is the number of atoms considered.

References

[1] Sakurai T and Hagstrum H 1976 *Phys. Rev.* B **14** 1593
[2] Chabal Y J, Chaban E E and Christman S B 1983 *J. Electron Spectrosc. Relat. Phenom.* **29** 35
Chabal Y J 1986 *Surf. Sci.* **168** 594

[3] Stucki F, Schaefer J A, Anderson J R, Lapeyre G J and Göpel W 1983 *Solid St. Commun.* **47** 795
[4] Tully J C, Chabal Y J, Raghavachari K, Bowman J M and Lucchese R R 1985 *Phys. Rev.* B **31** 1184
Lucchese R R and Tully J C 1983 *Surf. Sci.* **137** 570
[5] Stillinger F H and Weber T A 1984 *Phys. Rev.* B **31** 5262
[6] Selmani A, Salahub D R and Yelon A 1988 *Surf. Sci.* **202** 269
[7] Nosé S 1984 *Mol. Phys.* **52** 255
[8] Hoover W G 1985 *Phys. Rev.* A **31** 1695
[9] Biswas R and Hamann D R 1985 *Phys. Rev. Lett.* **55** 2001
[10] Weber T A 1985 *Mater. Res. Soc. Symp. Proc.* **63** 163
[11] Abraham F and Batra P 1985 *Surf. Sci. Lett.* **163** L752
[12] McQuarrie D A 1976 *Statistical Mechanics* ed. S A Rice (New York: Harper & Row)
[13] Berens P H and Wilson K 1981 *J. Chem. Phys.* **74** 4872
[14] Alben R, Weaire D, Smith J E Jr and Brodsky M H 1975 *Phys. Rev.* B **11** 2271
[15] Winer K 1987 *Phys. Rev.* B **35** 2366
[16] Berger J, Selmani A, Tannous C and Spronken G 1988 *Surf. Sci.* **202** 255
[17] Ralston A and Rabinowitz P 1978 *A First Course in Numerical Analysis* 2nd edn (New York: McGraw-Hill) p 191
[18] Chabal Y J and Raghavachari K 1984 *Phys. Rev. Lett.* **53** 282
[19] Tubino R, Piseri L and Zerbi G 1972 *J. Chem. Phys.* **56** 1022
[20] Beeman D 1976 *J. Comp. Phys.* **20** 130
[21] Jang J, Lee C G, Park S C and Lee C 1987 *Appl. Phys. Lett.* **51** 1673
[22] Dunlap B I, Connolly J W D and Sabin J R 1979 *J. Chem. Phys.* **71** 3396
[23] Vosko S H, Wilk L and Nusair M 1980 *Can. J. Phys.* **58** 1200
[24] Appelbaum J A and Hamann D R 1977 *Phys. Rev.* B **15** 2006